CRANK-NICOLSON GALERKIN MODEL FOR NONLINEARLY COUPLED MACROPHASE AND MICROPHASE TRANSPORT IN THE SUBSURFACE

By

AMENA MOTH MAYENNA

A thesis submitted in partial fulfillment of

the requirements for the degree of

Masters of Science in Environmental Engineering

WASHINGTON STATE UNIVERSITY
Department of Civil and Environmental Engineering

AUGUST 2008

To the Faculty of Washington State University:

The members of the Committee appointed to examine the thesis of AMENA MOTH MAYENNA find it satisfactory and recommend that it be accepted.

_____
Chair

_____

_____

ACKNOWLEDGEMENTS

First of all I would like to thank Dr. Akram Hossain for his aid in developing this thesis. His extensive knowledge, extreme patience and willingness to help were and are greatly appreciated.

Next I thank the members of my reading committee for their time and energy in helping me improve this document: Dr. Ken Hartz, Dr. James B. Duncan.

I acknowledge, appreciate, and return the love and support of my family, without whom I would be lost. My parents have been my emotional anchors through not only the vagaries of graduate school, but my entire life. Last of all I would like to thank Nazmul Hasan for his great support and help throughout the entire work.

CRANK-NICOLSON GALERKIN MODEL FOR NONLINEARLY COUPLED MACROPHASE AND MICROPHASE TRANSPORT IN THE SUBSURFACE

Abstract

by AMENA MOTH MAYENNA,
Washington State University
AUGUST 2008

Chair: Akram Hossain.

The subsurface can be considered to consist of two phases - the macrophase and the microphase in the context of contaminant transport. The interparticle pore spaces constitute the macrophase with the intraparticle pore spaces constituting the microphase. The macrophase transport is, often times, nonlinearly coupled with the microphase transport. The solution of nonlinearly coupled macrophase and microphase transport is particularly challenging. A Crank-Nicolson Galerkin finite element model (CNGFEM) has been developed to simulate the macrophase transport nonlinearly coupled with the microphase transport. The model is stable and provides oscillation-free results when the mesh Peclet number $Pe_m \leq 2.5$ and the Courant number $Cr \approx 1$. The model predictions were also found to be in excellent agreement with experimental data obtained from literature.

TABLE OF CONTENTS

Page

LIST OF TABLES

LIST OF FIGURES

INTRODUCTION

The subsurface can be considered to consist of two phases in the context of contaminant transport. The phases are the macrophase comprising of interparticle pore spaces and the microphase comprising of intraparticle pore spaces. Contaminants are transported mainly by advection and dispersion through the macrophase. Sorption and reaction can significantly impact the transport process. Slow sorption of contaminants in the subsurface has been successfully simulated by employing intraparticle diffusion models (Crittenden et al., 1986; Haggerty and Gorelick, 1995; Cunningham et al., 1997; Kleineidam et al., 1999).

Sorption isotherm, that relates water phase contaminant concentration with that of the adsorbed phase, are specific to the contaminant of concern for a given soil and can be linear or nonlinear (Xing and Pignatello, 1997; Xia and Ball, 2000). Linear isotherms are easy to implement in a numerical model. Nonlinear isotherms, however, can add to the challenge and complexity of solving coupled macrophase and microphase transport equations.

Leidl and Ptak (2003) modified the modular solute transport model in 3-dimension (MT3D) developed by Zheng (1990) to simulate coupled macrophase and microphase transport in the subsurface. The modification was implemented by developing a finite difference model (FDM). The FDM, however, requires strict conditions for stability and, often times, leads to oscillatory solutions resulting in negative concentrations and numerical instability. Liang (1984) presented a FDM for simulating nonlinearly coupled macrophase and microphase transport of contaminants in a fixed bed of activated carbon. An examination of the

FORTRAN program listing presented by Liang (1984) reveals that the model might have suffered from oscillation resulting in negative contaminant concentrations leading to numerical instability. Negative concentration is a physical impossibility and is normally avoided by setting it to zero arbitrarily (Hossain and Yonge, 1992).

The method of orthogonal collocation (MOC) is also frequently employed in solving coupled macrophase and microphase transport equations. The MOC is reported to fail due to numerical oscillations (Thibaud-Erkey et al., 1996). Thacker (1981) presented an excellent model to simulate transport of contaminants through a packed bed of activated carbon. The model was developed by employing the MOC. An inspection of the FORTRAN program listing presented by Thacker (1981) appears to suggest that the model might have suffered from numerical instability due to oscillatory results. Further, it is difficult to extend the MOC to field scale modeling.

Hossain and Yonge (1992) conclude that finite element models (FEMs) are better than the FDM and the MOC with regard to convergence and stability. Hossain and Yonge (1992) presented an "upwind" Galerkin FEM (GFEM) to simulate advective transport of contaminants through activated carbon columns. The model did not, however, include the effect of dispersion and reaction, and was first-order in time. Further, upwinding is known to introduce artificial dispersion.

Noorishad et al. (1992) reported that Crank-Nicolson time stepping, when used in

conjunction with the GFEM, provides higher order temporal accuracy to simulate advective-dispersive transport. Perrochet and Be´rod (1993) have shown that the Crank-Nicolson GFEM (CNGFEM) should provide accurate results for $Pe_m Cr \leq 2$ where Pe_m is the mesh Peclet number and Cr is the Courant number.

Therefore, the objective of this paper is to present a CNGFEM to simulate nonlinearly coupled macrophase and microphase transport in the subsurface. Additionally, the paper explores stability of the model and compares model predictions with experimental data obtained from literature.

MODEL EQUATIONS

The model equations can be derived by applying the principle of mass balance with the assumption that the soil particles are spherical. The model equations are given below even though they can be found elsewhere (Lee et al., 2007; Thacker, 1981).

$$\frac{\partial C}{\partial t} = -v\frac{\partial C}{\partial x} + D\frac{\partial^2 C}{\partial x^2} - 3\frac{k_f}{R}\frac{1-\varepsilon}{\varepsilon}(C - C_s) - \lambda C \quad (1)$$

$$\frac{\partial q}{\partial t} = \frac{D_s}{r^2}\frac{\partial}{\partial r}\left(r^2\frac{\partial q}{\partial r}\right) \quad (2)$$

In the above equations, C is the macrophase concentration of the contaminant (ML^{-3}), t is the time (T), v is the velocity of flow through the macrophase (LT^{-1}), x is the length of the flow field (L), D is the dispersion coefficient (L^2T^{-1}), k_f is the film transfer coefficient

(LT^{-1}), R is the radius of a particle (L), ε is the macrophase porosity, C_s is the concentration of contaminants in the boundary layer surrounding a particle (ML^{-3}), λ is the first-order reaction rate constant (T^{-1}), q is the adsorbed phase contaminant concentration (MM^{-1}), D_s is the microphase diffusion coefficient (L^2T^{-1}), and r is the radial distance from the center of a particle (L).

Eq. 1 describes transport in the macrophase and can be subjected to the following initial and boundary conditions.

$$t = 0, \quad 0 < x \le L, \quad C = C_0(x) \tag{3}$$

$$t \ge 0, \quad x = 0, \quad C = C_0 \tag{4}$$

$$t \ge 0, \quad x = L, \quad \frac{\partial C}{\partial x} = 0 \tag{5}$$

In the above equations, L is the length of the domain to be simulated, $C_0(x)$ is the initial concentration, and C_0 is contaminant concentration at the upstream boundary.

Eq. 2 describes transport of contaminants in the microphase. It can be subjected to the following initial and boundary conditions.

$$t = 0 \quad 0 \le r < R, \quad q = 0 \tag{6}$$

$$t \ge 0, \quad r = 0, \quad \frac{\partial q}{\partial r} = 0 \tag{7}$$

$$t \ge 0, \quad r = R, \quad D_s \rho \frac{\partial q}{\partial r} = k_f (C - C_s) \tag{8}$$

In the above equations, ρ is the bulk density of the soil $\left(ML^{-3}\right)$. The water phase concentration of the contaminant, C_s, in the boundary layer is assumed to be in equilibrium with the solid phase concentration q_s and the equilibrium relationship can be expressed by the following isotherm equation.

$$q_s = kC_s^{\,n} \tag{9}$$

Here k and n are constants specific to the soil and the contaminant of concern.

NONDIMENSIONAL MODEL EQUATIONS

The model equations were converted to their respective nondimensional forms by introducing the following dimensionless variables to minimize computational difficulty inherent to the solution of coupled micro- and macrophase transport equations.

$$\overline{C} = \frac{C}{C_0};\quad \overline{C}_s = \frac{C_s}{C_0};\quad \overline{q} = \frac{q}{q_e} \tag{10 – 12}$$

$$\overline{x} = \frac{x}{L};\quad \overline{r} = \frac{r}{R};\quad \tau = \frac{L}{v} \tag{13 – 15}$$

$$D_g = \rho\frac{q_e}{C_0}\frac{1-\varepsilon}{\varepsilon};\quad \overline{t} = \frac{t}{\tau D_g};\quad Pe = \frac{vL}{D} \tag{16 – 18}$$

$$St = \frac{k_f\tau(1-\varepsilon)}{\varepsilon R};\quad Sr = \lambda\tau D_g;\quad E_d = \frac{\tau D_g D_s}{R^2} \tag{19 – 21}$$

$$Sh = \frac{Rk_fC_0}{D_s\rho q_e} \tag{22}$$

Among the dimensionless variables, a few are of particular significance in the context of coupled macrophase and microphase transport. These are the solute distribution parameter D_g, the Peclet number Pe, the Stanton number St, the surface diffusion modulus E_d, and the Sherwood number Sh.

Eqs. 1 and 2 and the associated initial and boundary conditions were transformed to the following nondimensional forms by utilizing these variables.

$$\frac{\partial \overline{C}}{\partial \overline{t}} = -D_g \frac{\partial \overline{C}}{\partial \overline{x}} + \frac{D_g}{P_e} \frac{\partial^2 \overline{C}}{\partial \overline{x}^2} - 3D_g St(\overline{C} - \overline{C}_s) - Sr\overline{C} \tag{23}$$

$$\overline{r}^2 \frac{\partial \overline{q}}{\partial \overline{t}} = E_d \frac{\partial}{\partial \overline{r}} \left[\overline{r}^2 \frac{\partial \overline{q}}{\partial \overline{r}} \right] \tag{24}$$

$$\overline{t} = 0, \quad 0 < \overline{x} \le 1, \quad \overline{C} = \overline{C}_0(\overline{x}) \tag{25}$$

$$\overline{t} \ge 0, \quad \overline{x} = 0, \quad \overline{C} = 1.0 \tag{26}$$

$$\overline{t} \ge 0, \quad \overline{x} = 1, \quad \frac{\partial \overline{C}}{\partial \overline{x}} = 0 \tag{27}$$

$$\overline{t} = 0 \quad 0 \le \overline{r} < 1, \quad \overline{q} = 0 \tag{28}$$

$$\overline{t} \ge 0, \quad \overline{r} = 0, \quad \frac{\partial \overline{q}}{\partial \overline{r}} = 0 \tag{29}$$

$$\overline{t} \ge 0, \quad \overline{r} = 1, \quad \frac{\partial \overline{q}}{\partial \overline{r}} = Sh(\overline{C} - \overline{C}_s) \tag{30}$$

$$\overline{r} = 1, \quad \overline{q}_s = \overline{C}_s^{\,n} \tag{31}$$

SOLUTION TECHNIQUE

Piece-wise linear basis functions (PLBFs) were utilized to discretize the model equations for

computational simplicity. Application of the Crank-Nicolson time stepping scheme and the Galerkin minimization principle to Eq. 23, the macrophase transport equation, led to the derivation of the following system of ordinary differential equations (ODEs) in time.

$$\begin{aligned}[A]\left\{\frac{d\bar{C}}{d\bar{t}}\right\}+\frac{D_g}{2}[A^a]\{\bar{C}\}^k+\frac{D_g}{2P_e}[A^d]\{\bar{C}\}^k+3D_gSt[A]\{\bar{C}\}^k+Sr[A]\{\bar{C}\}^k \\ =\{E\}-\frac{D_g}{2}[A^a]\{\bar{C}\}^{k-1}-\frac{D_g}{2P_e}[A^d]\{\bar{C}\}^{k-1}+3D_gSt[A^s]\{\bar{C}_s\}^{k-1}\end{aligned} \tag{32}$$

An excellent treatment of the Galerkin principle and the PLBFs can be found elsewhere (Lapidus and Pinder, 1982). Matrices and vectors in the preceding equation are defined below.

$$a_{ij}=\int\varphi_i(\bar{x})\varphi_j(\bar{x})d\bar{x} \qquad i,j=1,2,3,...,NA \tag{33}$$

$$a_{ij}^a=\int\frac{d\varphi_i(\bar{x})}{d\bar{x}}\varphi_j(\bar{x})d\bar{x} \qquad i,j=1,2,3,...,NA \tag{34}$$

$$a_{ij}^d=\int\frac{d\varphi_i(\bar{x})}{d\bar{x}}\frac{d\varphi_j(\bar{x})}{dx}d\bar{x} \qquad i,j=1,2,3,...,NA \tag{35}$$

$$a_{ij}^s=\begin{cases}0 & i\neq j\\ \int\varphi_i(\bar{x})d\bar{x} & i=j\end{cases} \tag{36}$$

$$\{E\}=\{e_1 \quad 0 \quad 0 \quad \cdot \quad \cdot \quad 0 \quad 0\}^T \tag{37}$$

$$e_1=\left(\frac{1}{2}D_g+\frac{D_g}{P_e}\frac{1}{\Delta\bar{x}}\right)\left(\bar{C}_0^k+\bar{C}_0^{k-1}\right)-3D_gSt\frac{\Delta\bar{x}}{6}\bar{C}_0^k-\lambda\tau D_g\frac{\Delta\bar{x}}{6}\bar{C}_0^k \tag{38}$$

The matrices and the vector in the preceding equations are of dimensions $NA\times NA$ and $NA\times 1$, respectively, with NA being the number of finite elements of length $\Delta\bar{x}$.

The microphase transport equation was similarly discretized to obtain the following system of ODEs in time.

$$\left[P^{L}\right]\left\{\frac{d\bar{q}}{d\bar{t}}\right\} - E_d\left[P^{R}\right]\left\{\bar{q}^{k}\right\} = \left\{E_p\right\} \tag{39}$$

Elements of matrices and vectors in the preceding equation are defined below.

$$p_{ij}^{L} = \int \bar{r}^2 \varphi_i(\bar{r})\varphi_j(\bar{r})d\bar{r} \qquad i, j = 1,2,3,....NR \tag{40}$$

$$p_{ij}^{R} = \int \bar{r}^2 \frac{\varphi_i(\bar{r})}{d\bar{r}}\frac{\varphi_j(\bar{r})}{d\bar{r}}d\bar{r} \qquad i, j = 1,2,3,....NR \tag{41}$$

$$\left\{E_p\right\} = \left\{0 \quad \cdot \quad \cdot \quad 0 \quad e_{NR}\right\}^{T} \tag{42}$$

$$e_{NR} = E_d Sh\left(\bar{C} - \bar{C}_S\right) \tag{43}$$

The matrices in the preceding equations are of dimension $NR \times NR$. The vectors are of dimension NR with $NR-1$ being the number of radial finite elements of length $\Delta\bar{r}$.

Implicit backward discretization of the temporal derivatives in Eqs. 32 and 39 followed by some mathematical manipulation resulted in the following sets of algebraic equations.

$$\left[L^{G}\right]\left\{\bar{C}^{k}\right\} = \left[L^{R}\right]\left\{\bar{C}^{k-1}\right\} + \Delta\bar{t}\left\{E\right\} + 3D_g St\Delta\bar{t}\left[A^{s}\right]\left\{\bar{C}_s^{k-1}\right\} \tag{44}$$

$$\left[S^{G}\right]\left\{\bar{q}^{k}\right\} = \left[P^{L}\right]\left\{\bar{q}^{k-1}\right\} + \Delta\bar{t}\left\{E_p\right\} \tag{45}$$

In the above equations:

$$\left[L^G\right] = \left(1 + 3D_g St\bar{\Delta t} + Sr\bar{\Delta t}\right)\left[A\right] + \frac{D_g}{2}\bar{\Delta t}\left[A^a\right] + \frac{D_g}{2Pe}\bar{\Delta t}\left[A^d\right] \quad (46)$$

$$\left[L^R\right] = \left[A\right] - \left(\frac{D_g\bar{\Delta t}}{2}\left[A^a\right] + \frac{D_g\bar{\Delta t}}{2Pe}\left[A^d\right]\right) \quad (47)$$

$$\left[S^G\right] = \left[P^L\right] - E_d\bar{\Delta t}\left[P^R\right] \quad (48)$$

The matrices $\left[L^G\right]$ and $\left[S^G\right]$ are constant and do not change with time. The matrices were decomposed into upper and lower triangular matrices by applying the LU decomposition principle (Burden and Faires, 1993). At each time step, the systems of Eqs. 44 and 45 were solved by forward and backward substitutions. Eq. 44 was solved first. Values of $\overline{C}$ obtained from Eq. 44 were used while solving Eq. 45 to find microphase concentrations $\overline{q}$. Concentration $\overline{C}_s$ at a given node for the water phase was computed by employing Eq. 49 given below.

$$\overline{C}_s = \left(\overline{q}_{NR}\right)^{1/n} \quad (49)$$

STABILITY ANALYSIS

Stability analysis was performed by employing the von Neumann principle. The model was found to be stable for $Pe_m \leq 2.5$ and $Cr \approx 1.0$. Stability based on the von Neumann principle does not always ensure oscillation-free results. Oscillation in the solution of the

macrophase equation may lead to negative concentrations, which is a physical impossibility. Eigenvalues of amplification matrices for the two phases can be considered better indicators of oscillation-free results. It was observed that as the imaginary components of the eigenvalues get larger, oscillation becomes more pronounced. Numerical experiments, conducted by utilizing parameters contained in Table 1, revealed that the imaginary components of the macrophase eigenvalues were the smallest for $Cr \approx 1.0$ when $Pe_m \leq 2.50$. The eigenvalues for the microphase were all real and less than unity. Therefore, the model can be expected to provide oscillation-free results for $Pe_m \leq 2.5$ and $Cr \approx 1.0$ for a system with parameter values similar to those listed in Table 1.

EFFECT OF ADSORPTION PARAMETERS

Fig. 1 presents concentration at the downstream boundary, $\overline{C}_e$, as a function of $\bar{t}$ to show the effect of adsorption parameters on model predictions. Adsorption data for three organic compounds onto soil were obtained from literature (Xing and Pignatello, 1998) for this analysis. The compounds are vanillic acid (VA) with $k = 14.3\,\mu g\,g^{-1}\left(\mu g\,mL^{-1}\right)^{-0.576}$ and $n = 0.576$, trans-cinnamic acid (TCA) with $k = 130.0\,\mu g\,g^{-1}\left(\mu g\,mL^{-1}\right)^{-0.673}$ and $n = 0.673$, and 2,4-dichlorobenzene (2,4-DCP) with $k = 360.0\,\mu g\,g^{-1}\left(\mu g\,mL^{-1}\right)^{-0.761}$ and $n = 0.761$.

VA adsorption onto soil can be considered the weakest among the three compounds. Weak adsorption results in low retardation. Consequently, VA is transported faster and arrives at the downstream boundary the earliest as shown in Fig. 1. Furthermore, concentration of VA at the downstream boundary gradually rises to the steady state concentration of unity. TCA

adsorption is stronger than VA as evident from the magnitudes of its adsorption parameters and, therefore, arrive at the downstream boundary later. 2,4-DCP arrives at the downstream boundary even later for it is partitioned more onto soil. Therefore, stronger adsorption leads to higher retardation and slower transport velocity of the contaminant for a given set of film transfer and intraparticle diffusion coefficients. Furthermore, concentration at the downstream boundary rises rapidly to the steady state concentration for compounds with strong adsorption.

EFFECT OF TRANSPORT PARAMETERS

Effect of transport parameters on model predictions was investigated for $NA = 200$, $NR = 5$, and $\Delta\bar{t} = 5.0\times10^{-6}$ which corresponds to $Pe_m = 2.5$ and $Cr \approx 1.0$. Transport parameters of interest are v, D, k_f, and D_s. As expected, larger v causes the contaminant to move faster and consequently, an earlier arrival of the contaminant at the downstream boundary was predicted. An increase in D is reflected in the increased smearing of $\overline{C}_e$ vs. $\bar{t}$ curve. Effect of varying film transfer coefficient, k_f, on the temporal distribution of $\overline{C}_e$ is presented in Fig. 2. The film transfer coefficient was varied from 1.0×10^{-4} to 1.0×10^{-3} cm s^{-1} with an intermediate value of 5.0×10^{-4} cm s^{-1}. Smaller k_f reduces transfer of contaminants onto the particle surfaces causing reduced adsorption and smaller retardation. Consequently, the contaminant arrives at the downstream boundary the earliest for the smallest k_f of 1.0×10^{-4} cm s^{-1}. However, as k_f is increased, a limiting point is reached for a given D_s such that diffusion into the solid particles and consequently, adsorption onto the particle surfaces is controlled by D_s. An increase of k_f to

5.0×10^{-4} cm s^{-1} and beyond seems to indicate such a limiting point for a diffusion coefficient of 1.0×10^{-9} cm^2 s^{-1} as evident from Fig. 2.

Fig. 3 presents $\overline{C}_e$ as a function of $\bar{t}$ for varying diffusion coefficient D_s. Diffusion coefficient was varied from 1.0×10^{-10} to 1.0×10^{-8} cm^2 s^{-1} with an intermediate value of 1.0×10^{-9} cm^2 s^{-1}. As the diffusion coefficient is increased, a limiting point is reached when contaminant transport into the particle is controlled by the film transfer coefficient. An examination of Fig. 3 indicates that for $k_f = 1.0\times10^{-3}$ cm s^{-1}, the limiting point is reached for $D_s = 1.0\times10^{-9}$ cm^2 s^{-1}. Therefore, further increase in D_s does not appear to have noticeable effect on adsorption and hence retardation.

MODEL PREDICTION VERSUS EXPERIMENTAL DATA

Adsorption

Single-solute breakthrough curves (BTCs) for 2-methyl-4,6-dinitrophenol (2-M-4,6-DNP) and 2,4,6-trichlorophenol (2,4,6-TCP) for soil columns of height 50 cm were obtained from Rahman et al. (2003). Model parameters were also obtained from Rahman et al. (2003) and are summarized in Table 2. Fig. 4 presents a comparison between the model prediction and the experimental data for 2-M-4,6-DNP. The model prediction is found to be in excellent agreement with the experimental data. Similar observation is also made for 2,4,6-TCP based on the comparison presented in Fig. 5.

Experimental BTCs for dibenzothiophene (DBT) and pentachlorophenol (PCP) and associated parameters were obtained from Worch (2004). Model parameters for DBT and

PCP are also listed in Table 2. Comparisons of model predictions and experimental BTCs for DBT and PCP are presented in Figs. 6 and 7, respectively. An examination of the figures reveals excellent agreements between the model predictions and the experimental results.

2-M-4,6-DNP and 2,4,6-TCP are relatively less hydrophobic than DBT and PCP as evident from their respective adsorption constant k. Mass transfer Biot numbers (Bi) were calculated for all the solutes and were found to be in the range of 85 – 1425. A Bi of greater than or, equal to 30 is normally considered a diffusion controlled transport (Weber and Digiano, 1996).

Adsorption followed by Desorption

Experimental BTCs for adsorption followed by desorption for simazine was obtained from Suárez et al. (2007). Model parameters listed in Table 2 for this compound was also obtained from literature (Suárez et al., 2007) except k_f and D_s that were computed by employing empirical correlation reported by Worch (2004).

Fig. 8 presents a comparison of model prediction with experimental data for simazine. An excellent agreement between model prediction and experimental data is evident from the figure for adsorption parameter $k = 1.24\ \text{mL g}^{-1}$. Suárez et al. (2007) reports a range of $0.263 – 2.156\ \text{mL g}^{-1}$ for k. Simazine is significantly hydrophobic. A Bi of approximately 5.0 was computed for simazine.

CONCLUSIONS

The finite element model, CNGFEM, developed can simulate coupled macrophase and microphase transport in the subsurface effectively. The model is stable and provides oscillation-free results when $Pe_m \leq 2.5$ and $Cr \approx 1.0$. The model predictions are found to be in excellent agreements with the experimental data for a wide range of system conditions.

REFERENCES

Burden, L.R. and Faires, J.D., Direct method for solving linear systems, Numerical Analysis, PWS-KENT Publishing Company, Boston, MA., pp. 366-369, 1993.

Crittenden, J.C., Hutzler, N.J., Geyer, D.G., Oravitz, J.L. and Friedman, G., Transport of organic compounds with saturated groundwater flow: Model development and parameter sensitivity, Water Resour. Res., vol. 22 (3), pp. 271-284, 1986.

Cunningham, J.A., Werth, C.J., Reinhard, M. and Roberts, P.V., Effects of grain-scale mass transfer on the transport of volatile organics through sediments, 1, Model development, Water Resour. Res., vol. 33(12), pp. 2713-2726, 1997.

Haggerty, R. and Gorelick, S.M., Multiple rate mass-transfer for modeling diffusion and surface reactions in media with pore-scale heterogeneity, Water Resour. Res., vol. 31(10), pp. 2383-2400, 1995.

Hossain, M.A. and Yonge, D.R., Finite element modeling of single-solute activated-carbon adsorption, J. Envir. Engrg., ASCE, vol. 118(2), pp. 238 – 252, 1992.

Kleineidam, S., Runger, H., Ligouis, B. and Grathwohl, P., Organic matter facies and equilibrium sorption of phenanthrene, Environ. Sci. Technol., vol. 33, pp. 1637-1644, 1999.

Lapidus, L. and Pinder, F. G., Numerical solution of partial differential equations in science and engineering, Wiley, New York, U.S.A., 1982.

Lee, J. W., Yang, T. H., Shim, W. G., Kwon, T. O. and Moon, I. S., Equilibria and dynamics of liquid-phase trinitrotoluene adsorption on granular activated carbon: Effect of temperature and pH, J. Haz. Mat., vol. 141, pp.185-192, 2007.

Liang, S., Mathematical modeling of sorption in heterogeneous system. Ph. D. Dissertation, University of Michigan, Ann Arbor, Michigan, U.S.A. 1984.

Liedl, R. and Ptak, T., Modeling diffusion-limited retardation of contaminants in hydraulically and lithologically nonuniform media, J. Contam. Hydrol., vol. 66, pp. 239-259, 2003.

Noorishad, J., Tsang, C.F., Perrochet, P. and Musy, A., A perspective on the numerical solution of convection dominated transport problems: a price to pay for easy way out, Water

Resour. Res., vol. 28(2), pp. 551-561, 1992.

Perrochet, P. and Be´rod, D., Stability of the standard Crank-Nicolson-Galerkin scheme applied to the diffusion-convection equation: some new insights, Water Resour. Res., vol. 28, pp. 3291-3297, 1993.

Rahman, M., Amiri, F. and Worch, E., Application of the mass transfer model for describing nonequilibrium transport of HOCs through natural geosorbents,
Water Research., vol. 37, pp. 4673-4684, 2003.

Suárez F., Bachmann J., Muñoz J. F., Ortiz C., Tyler S. W., Alister C. and Kogan M., Transport of simazine in unsaturated sandy soil and predictions of its leaching under hypothetical field conditions, J. Contam. Hydrol., vol. 94, pp. 166 – 177, 2007.

Thacker, W.E., Modeling of activated carbon and coal gasification char adsorbents in single-solute and bisolute systems, Ph. D. Dissertation, University of Illinois at Urbana-Champaign, Urbana, Illinois, U.S.A. 1981.

Thibaud-Erkey, C.T., Guo, Y., Erkey, C. and Akgerman, A., Mathematical modeling of adsorption and desorption of volatile contaminants from soil: Influence of isotherm shape on adsorption and desorption profiles, Environ. Sci. Technol., vol. 30(7), pp. 2127-2134, 1996.

Weber, W. J., Jr. and Digiano, F.A., Process Dynamics in Environmental Systems.John Wiley & Sons, INC. New York, U.S.A. 1996.

Worch, E., Modeling the solute transport under nonequilibrium conditions on the basis of mass transfer equations, J. Contam. Hydrol., vol. 68, pp. 97 – 120, 2004.

Xia, G. and Ball, W.P., Polanyi-based models for the competitive sorption of low-polarity organic contaminants on a natural sorbent, Environ. Sci. Technol., vol. 34(7), pp. 1246-1253, 2000.

Xing, B. and Pignatello, J.J., Dual-mode sorption of low-polarity compounds in glassy poly (vinyl chloride) and soil organic matter, Environ. Sci. Technol., vol. 31(3), pp. 792–799, 1997.

Xing, B. and Pignatello, J.J., Competitive sorption between 1,3-dichlorobenzene or 2,4-dichlorophenol and natural aromatic acids in soil organic matter, Environ. Sci. Technol., vol. 32, pp. 614-619, 1998.

Zheng, C., MT3D., A modular three-dimensional transport model for simulation of advection, dispersion and chemical reaction of contaminants in groundwater systems, S.S. Papadopulos and Associates, Inc., Rockville, 1990.

TABLES

Table 1: Parameters used in stability analysis.

Parameter	Value
R	0.01 cm
ε	0.35
ρ_b	1.5 $g\,cm^{-3}$
k_f	$1.0\times10^{-3}\ cm\,s^{-1}$
D_s	$1.0\times10^{-9}\ cm^2\,s^{-1}$
k	$360\,\mu g\,g^{-1}\left(\mu g\,mL^{-1}\right)^{-0.761}$
n	0.761

Table 2: Parameters used in predicting BTCs to compare with experimental data.

Parameters	**2-M-4,6-DNP**	**2,4,6-TCP**	**DBT**	**PCP**	**Simazine**
$L\,(cm)$	50	50	50	50	10
$v\,(cm\,s^{-1})$	6.66×10^{-3}	6.66×10^{-3}	3.96×10^{-2}	1.68×10^{-2}	5.83×10^{-4}
$D\,(cm^2\,s^{-1})$	1.33×10^{-3}	1.33×10^{-3}	3.25×10^{-2}	1.34×10^{-2}	4.26×10^{-4}
$\rho_b\,(g\,cm^{-3})$	1.68	1.68	1.80	1.80	1.50
$r\,(cm)$	0.04	0.04	0.04	0.04	0.024
ε	0.37	0.37	0.32	0.33	0.31
$k\,(mL\,g^{-1})$	0.008	0.022	2.5	0.12	1.24
n	1	1	1	1	1
$C_0\,(mg\,L^{-1})$	0.10	0.10	0.0636	0.118	140
$k_f\,(cm\,s^{-1})$	1.47×10^{-3}	1.60×10^{-3}	2.27×10^{-3}	1.47×10^{-3}	5.06×10^{-4}
$D_s\,(cm^2\,s^{-1})$	1.92×10^{-6}	9.60×10^{-7}	1.60×10^{-7}	2.13×10^{-6}	8.57×10^{-7}

FIGURES

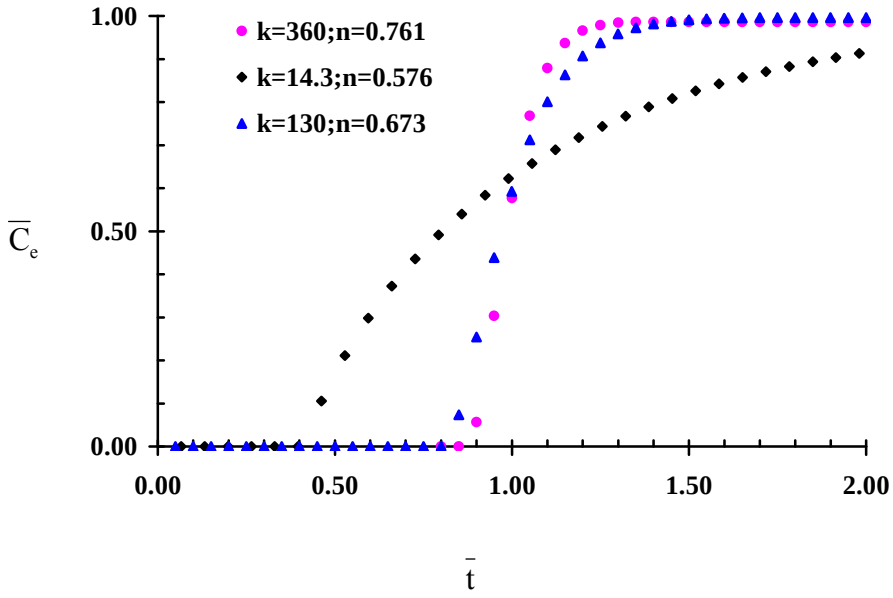

Fig. 1: Effect of adsorption parameters on model prediction.

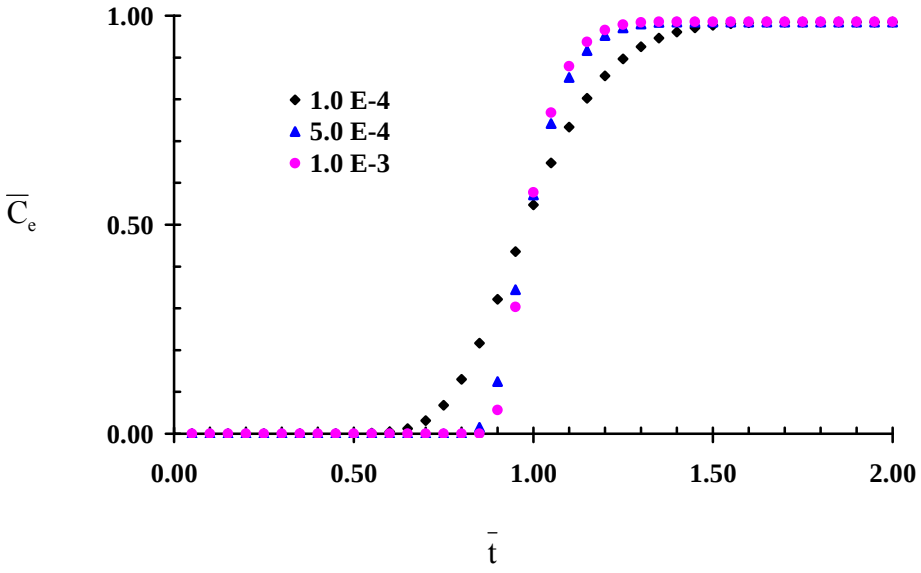

Fig. 2: Effect of varying film transfer coefficients, in $cm\ s^{-1}$, on model prediction.

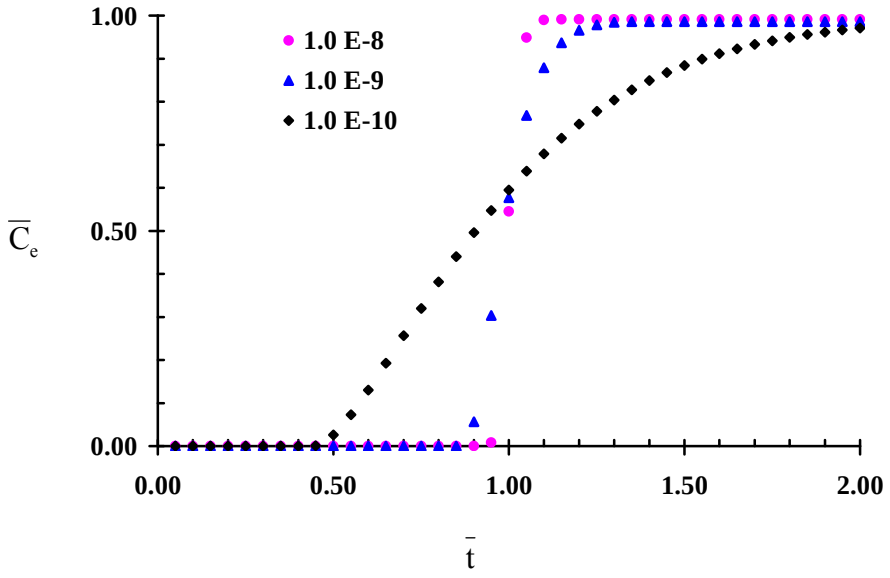

Fig. 3: Effect of varying diffusion coefficients, in $cm^2\ s^{-1}$, on model prediction.

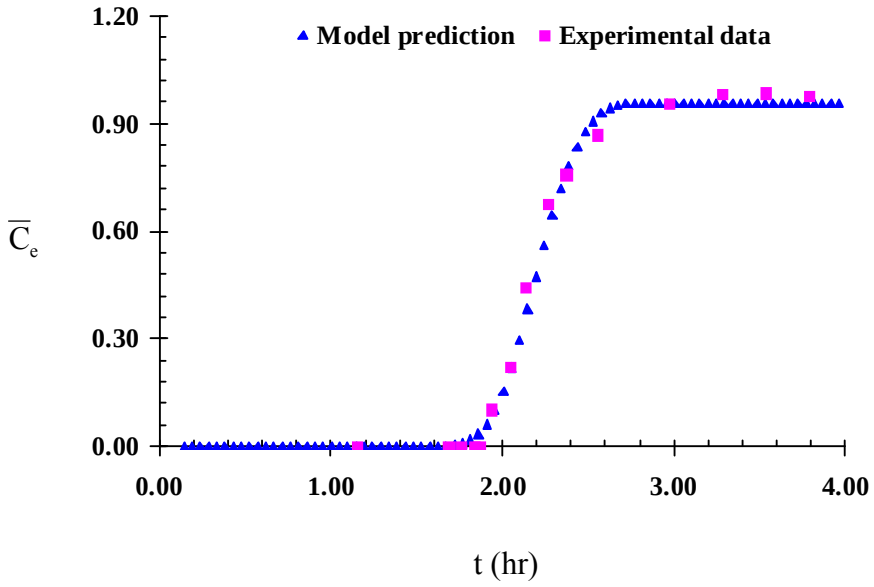

Fig. 4: Model predictions versus experimental results for 2-M-4,6-DNP obtained from Rahman et al. (2003).

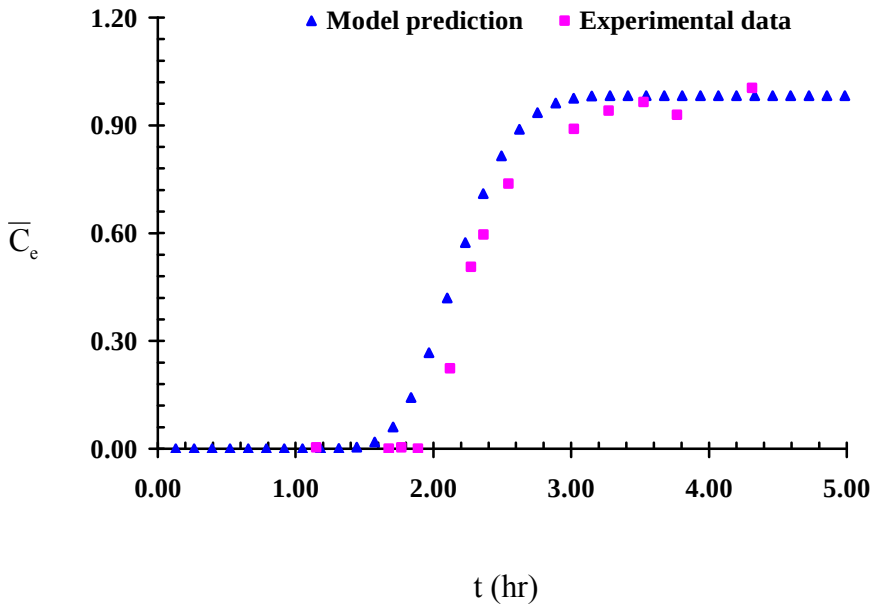

Fig. 5: Model predictions versus experimental results for 2,4,6-TCP obtained from Rahman et al. (2003).

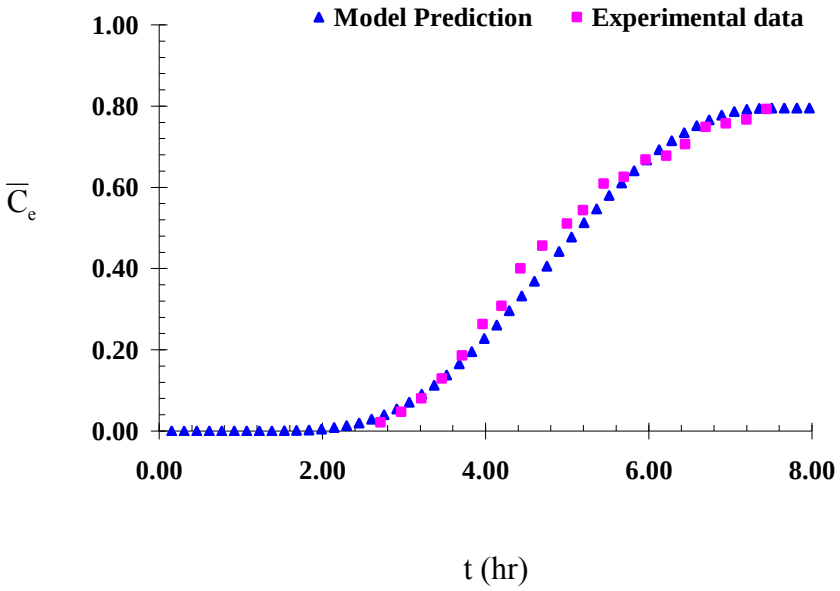

Fig. 6: Model predictions versus experimental results for DBT obtained from Worch (2004).

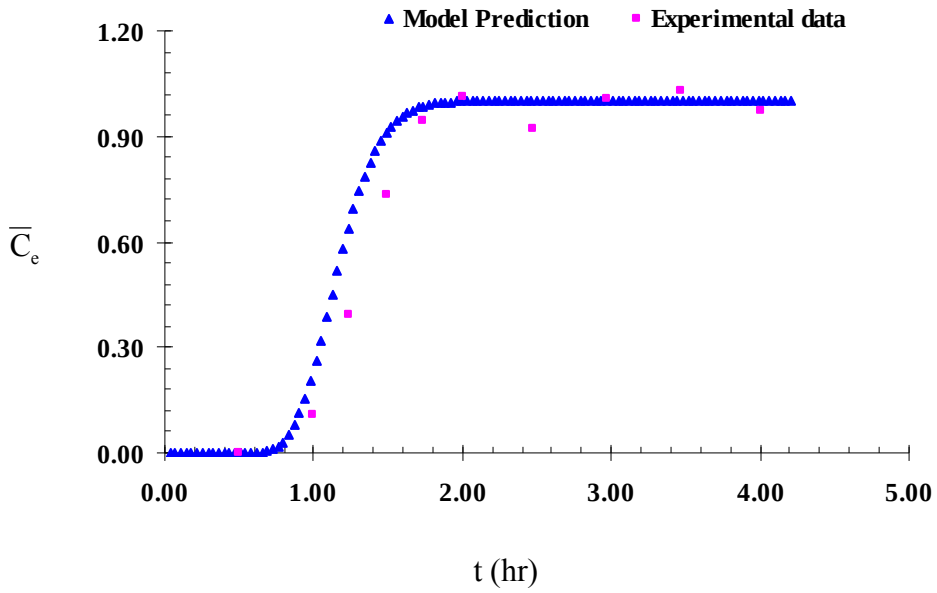

Fig. 7: Model predictions versus experimental results for PCP obtained from Worch (2004).

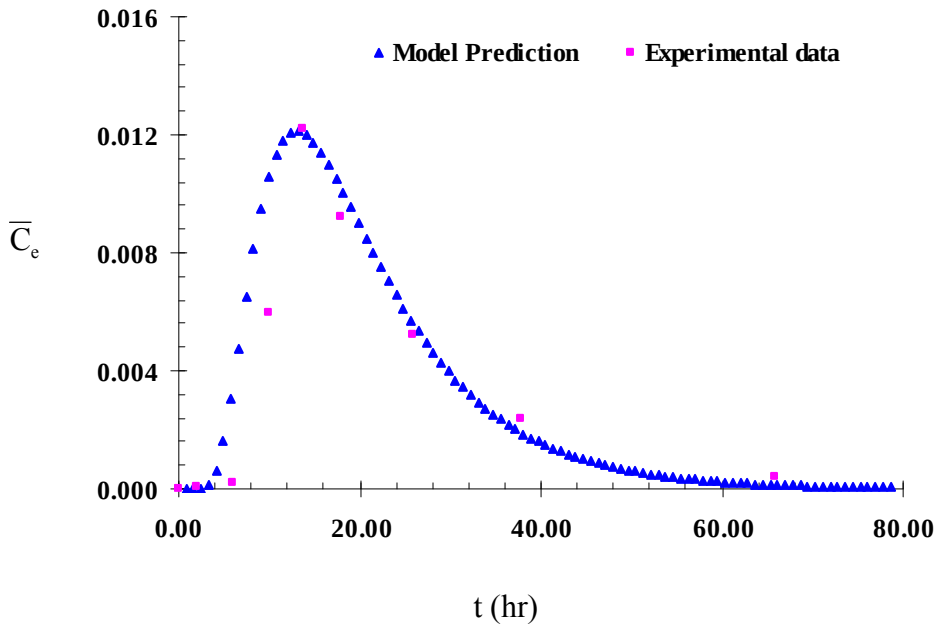

Fig. 8: Model predictions versus experimental results for simazine obtained from Suárez et al. (2007).

NOTATIONS

C = macrophase concentration of the contaminant (ML^{-3})

C_s = concentration of contaminants in the boundary layer surrounding a particle (ML^{-3})

$C_0(x)$ = initial concentration (ML^{-3})

C_0 = contaminant concentration at the upstream boundary (ML^{-3})

$\overline{C}$ = dimensionless macrophase concentration of the contaminant

$\overline{C}_s$ = dimensionless concentration of contaminants in the boundary layer

$\overline{C}_e$ = dimensionless concentration at the downstream boundary

D = dispersion coefficient (L^2T^{-1})

D_s = microphase diffusion coefficient (L^2T^{-1})

D_g = solute distribution parameter

E_d = surface diffusion modulus

k_f = film transfer coefficient (LT^{-1})

L = length of the domain to be simulated (L)

Pe = peclet number

q = adsorbed phase contaminant concentration (MM^{-1})

$\overline{q}$ = dimensionless microphase concentration of the contaminant

q_s = solid phase concentration in the boundary layer (ML^{-3})

R = radius of a particle (L)

r = radial distance from the center of a particle (L)

St = stanton number

Sh = sherwood number

t = time (T)

v = velocity of flow through the macrophase (LT^{-1})

x = length of the flow field (L)

ε = macrophase porosity

λ = first-order reaction rate constant (T^{-1})

ρ = bulk density of the soil (ML^{-3})